Numerical investigation of hypersonic boundary layers of perfect and dense gases

Luca Sciacovelli[1], Xavier Gloerfelt[1], Paola Cinnella[1], and Francesco Grasso[2]

[1] Arts et Métiers ParisTech, DynFluid Laboratory, Paris, France,
luca.sciacovelli@ensam.eu
[2] Conservatoire National des Arts et Métiers, DynFluid Laboratory, Paris, France

Abstract. Hypersonic turbulent boundary layers (HTBL) at Mach number M=6 of a dense gas (PP11) and a perfect gas (air) are investigated by means of Direct Numerical Simulations (DNS), from the laminar to fully turbulent state. The operating conditions are chosen in such a way to highlight dense gas effects, which profoundly alter the transition mechanisms and affect the turbulent flow properties significantly.

Keywords: Hypersonic flow, boundary layer, dense gas, DNS

1 Introduction

High-speed flows of gases with complex thermodynamic behavior (often referred-to as "real gases") have been paied growing interest from the scientific community due to the manifold applications in aerospace and power generation systems. In this work we focus on so-called dense gas flows found in several engineering applications, ranging from energy production to high-speed wind tunnels. Dense gases are single-phase fluids of complex molecules, at pressure and temperature conditions of the same order of their thermodynamic critical point. These fluids, in particular those belonging to the Bethe–Zeldovich–Thompson family, may exhibit nonclassical phenomena in the transonic and supersonic regimes such as expansion shocks or mixed waves; these nonclassical effects may be characterized by means of the fundamental derivative of gas dynamics Γ [1].

The influence of dense-gas effects on compressible turbulent flows has been previously investigated in isotropic turbulence [2, 3] and channel flow [4] configurations. Numerical simulations of hypersonic turbulent boundary layers (HTBL) enable the investigation of physical mechanisms characterizing a wall-bounded, non confined configuration. A fundamental question arising in high-Mach number flows concerns the laminar to turbulent transition. At hypersonic conditions higher instability modes of acoustic nature exist for air flows, as pointed out by Mack [5], leading to different mechanisms for instability growth and breakdown to turbulence, that must be understood in order to predict the transition location. Moreover, at these high flow speeds, the intricate coupling between thermal and dynamic effects, largely unexplored for the dense gas, affects the turbulent flow behavior and its contribution to skin friction and heat transfer.

In this work we investigate HTBL at external Mach number M=6 of a dense (DG) and a perfect gas (PFG) by means of Direct Numerical Simulations (DNS), from the laminar to fully turbulent state. The reference DNS considered for the purpose of comparison and validation for air is the HTBL investigated by Franko & Lele [6], who focused on the analysis of the transition mechanisms. A DG simulation is also conducted at the same Mach number. Although much higher than Mach numbers typically encountered in practical dense-gas applications, the chosen operating conditions are well suited to highlight dense gas effects.

2 Direct Numerical Simulation details

The selected working fluid for the dense gas case is a heavy fluorocarbon, namely PP11 ($C_{14}F_{24}$), previously considered for analyzing dense gas effects in different configurations [3, 4]. As in [4], the thermodynamic behavior of PP11 is modeled by the Martin-Hou equation of state and the variation of the transport properties with temperature and density is described by means of the Chung-Lee-Starling dense-gas model. DNS simulations are carried out by means of a ninth-order accurate numerical scheme (see [2]), supplemented by a non-linear artificial viscosity term equipped with a shock-capturing sensor described in [4].

The computational domain is defined from the plate leading edge and transition to turbulent is obtained by forcing the most unstable waves by means of suction and blowing. For the PFG boundary layer, we simulate an oblique breakdown scenario (modal transition), whereby the forcing excites the three-dimensional Tollmien-Schlichting mode (or first mode), as in the reference DNS of [6]. However, since our aim is to achieve fully turbulent conditions, a much longer computational domain and integration time are used with respect to [6].

For the DG case, a preliminary linear stability study was carried out to determine the 3D unstable spatial modes [7]. Contrary to PFG, DG velocity profiles are largely insensitive to the Mach number. Additionally, the temperature rise at the wall is less than 3% in this high-specific-heat fluid, whereas it is about 600% in the PFG. As a consequence, friction heating is almost suppressed and the velocity profile remains close to the incompressible one. Despite the apparently incompressible behavior, acoustic waves are present and deeply altered by the complex thermodynamics, which turns into dramatically different stability properties. In DG, the Tollmien-Schlichting mode disappears for Mach above ≈ 1.5, due to the absence of a generalized inflection point in the boundary layer profiles. This is unlike the classical behavior for air, whereby the appearance of a generalized inflection point tends to counteract the stabilizing effect of compressibility and sustains the first mode. An acoustic mode (or "Mack mode") appears for Mach numbers of 3 or higher. This mode becomes supersonic, thus capable of radiating acoustic waves, and it is characterized by a much higher frequency than the corresponding mode in PFG. Based on the stability study, we chose to excite the 2D acoustic mode maximizing the N factor at $Re_{\delta^*_{ref}} = 1200$, with $\omega\delta^*_{ref}/U_\infty = 0.6$ and an amplitude $\varepsilon = 0.02U_\infty$ to trigger transition in the dense gas boundary layer.

Table 1. Boundary layer properties and parameters.

Fluid	U_∞ [m/s]	ρ_∞ [kg/m^3]	T_∞ [K]	Re_θ	δ [mm]	θ [mm]	C_f $\times 10^3$	Δx^+	Δy_w^+	Δz^+	$N_x \times N_y \times N_z$
Air	969.7	0.13	65	5720	5.82	0.22	0.87	3.76	0.26	2.09	$7700 \times 300 \times 400$
PP11	198.8	348.411	646.8	4402	0.032	0.0029	2.13	8.12	0.65	9.77	$14336 \times 320 \times 280$

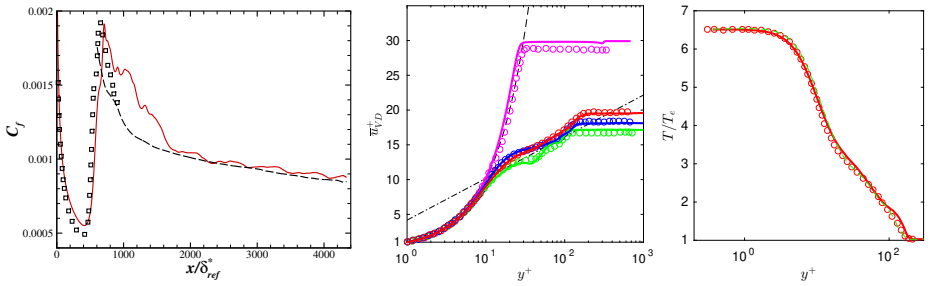

Fig. 1. Left: skin friction coefficient (— Present DNS; □ DNS of Franko & Lele; −− White's correlation). Center: mean streamwise velocity profiles for the present DNS (solid) and Franko&Lele (dashed) at locations x/δ^*_{ref}= 400 (—, ○), 650 (—, ○), 800 (—, ○), 950 (—, ○). Right: mean temperature profile at x/δ^*_{ref}=950 (— present DNS, ○ DNS of Franko & Lele, −− Walz's law).

Table 1 provides a summary of the reference conditions and numerical parameters for the perfect and dense gas DNS. In order to enhance dense-gas effects, the thermodynamic conditions for PP11 are chosen such that Γ is negative outside of the boundary layer, and remains lower than unity close to the wall. Moreover, for the chosen values of density and temperature, the speed of sound for PP11 is equal to c_∞=33.1 m/s, so that hypersonic conditions are achieved for much smaller velocities with respect to air, as shown in table 1. An isothermal condition is applied at the wall, with T_w = 422.5 K and 663.2 K for air and PP11, respectively, corresponding to the wall temperature for the laminar boundary layer (pseudo-adiabatic condition). The streamwise, wall-normal and spanwise resolutions, as well as properties of the boundary layer near the end of the computational domain, are summarized in table 1. The total number of grid points is of the order of $\sim 10^9$, with the dense-gas case having twice the number of points in the streamwise direction with respect to the air one.

3 Numerical results

PFG results are presented first. Comparisons are conducted in the transitional region, where DNS results for perfect gas are available (figure 1). The distribution of C_f matches the laminar correlation until x/δ^*_{ref}=400; then it rapidly departs from it and a significant overshoot is visible. The transition path and intensity of the overshoot are in very good agreement with Ref. [6]. Excellent agreement is also observed for the profiles of streamwise velocity and temperature. The mean temperature profiles closely follow Walz's law, confirming that pseudo-adiabatic conditions are obtained. A global view of the flow field for PFG is given in fig-

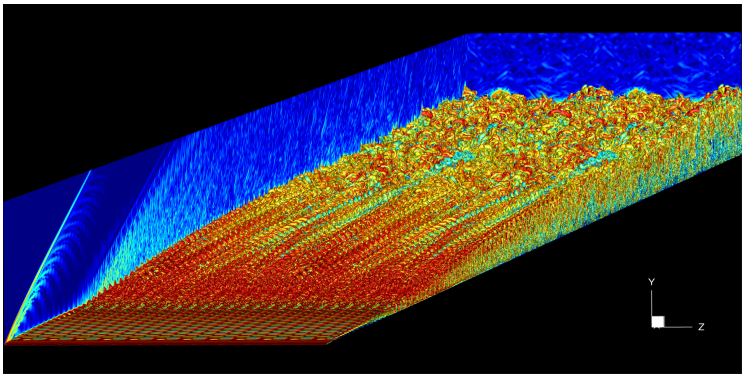

Fig. 2. Instantaneous views of the Q-criterion colored by the magnitude density gradient over the computational domain for the air HTBL.

ure 2, showing an iso-surface of the Q-criterion colored by the magnitude of the density gradient. The leading edge shock and the development of the unstable oblique waves downstream of the forcing strip is clearly visible, leading to the formation of an organized transition front and a transitional region characterized by long persistent streaky structures. A fully-turbulent state is reached in the last third of the computational domain. Results for DG are reported in figure 3 and compared with PFG. The DG skin friction distribution remains close to the incompressible one; the transition behavior is deeply modified, and no overshoot is observed. In this case, the transition region is governed by streaks that eventually break leading to turbulent spots instead of an organized front. It can also be noticed that, while the local momentum-thickness-based Reynolds numbers (Re_θ) are reasonably similar for both flows, their incompressible counterparts obtained by scaling with the ratio of the freestream to wall viscosity ($Re_{\theta,inc} = \mu_\infty/\overline{\mu}_w Re_\theta$) are very different due to the negligible friction heating in the DG.

Figure 4 shows selected first-order statistics profiles against the standard or semi-locally scaled wall coordinate at three stations ($Re_\theta = 2000$, 3000 and 4000) in the turbulent region. PFG is still transitional at the first station. For the DG velocity profile, the slope of the logarithmic region remains rather close to the incompressible case. Once again, the temperature variation across the boundary layer is very small. The density variation is also much smaller than in PFG (outer density is less than 1.25 times the wall density, instead of more than 6). Also note the peculiar variation of the viscosity, that follows the density variation and decreases when approaching the wall (liquid-like behavior).

Selected second-order statistics are reported in fig. 5. DG flow exhibits higher turbulent intensities, due to the higher local Reynolds number, and a dramatically different rms density profile. Compared to PFG, relative density fluctuations are much smaller and the fluctuation peak is located close to the wall and not in the outer region, as also observed in turbulent channel flow [4]. DG also reaches higher turbulent Mach numbers than PFG (not reported), with values

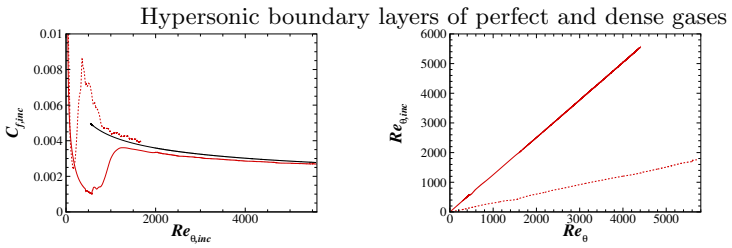

Fig. 3. Skin friction and Reynolds number distributions for DG (—) and PFG (−−).

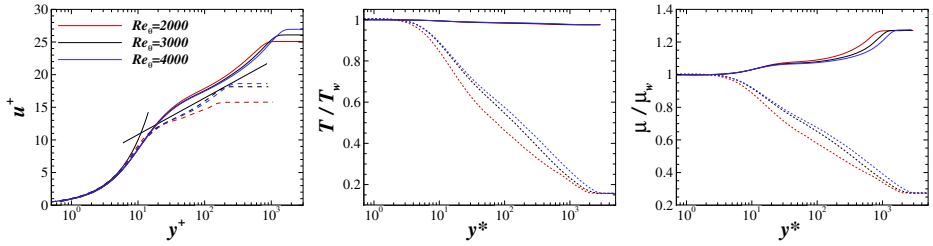

Fig. 4. Averaged profiles for PFG (−−) and DG (—) at various Reynolds numbers.

reached in the production peak region ($y^* \approx 12$) sufficiently high ($M_{t,\max} > 0.3$) for the potential formation of eddy shocklets. Even when turbulent Mach number is lower than such a threshold, the existence of eddy shocklets is not excluded [9], since instantaneous Mach number values can be much higher. In PFG, high rms Mach number values are encountered in the outer region, and indeed sheet-like structures corresponding to high density gradients and (mostly) strong compressions are observed in instantaneous Schlieren-like contours (fig. 6), while in DG the peak rms Mach number is located in the inner region. In this case, numerical Schlieren exhibit very high-density-gradient spots (corresponding to both strong compressions and expansions) located near the wall (in a region where the rms density is also at its maximum), whereas sheet-like structures in the outer region are more sporadic.

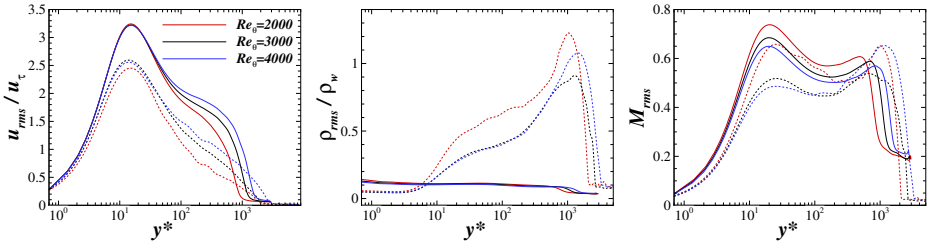

Fig. 5. Streamwise turbulent intensity (left), r.m.s. density (center) and r.m.s. Mach number (right) for PFG (−−) and DG (—) at various Reynolds numbers.

4 Conclusions and future work

Direct numerical simulations of hypersonic boundary layers including the laminar, transitional and fully turbulent regions were presented for perfect and dense gas at $M = 6$. For the dense gas, the complex thermodynamics and transport

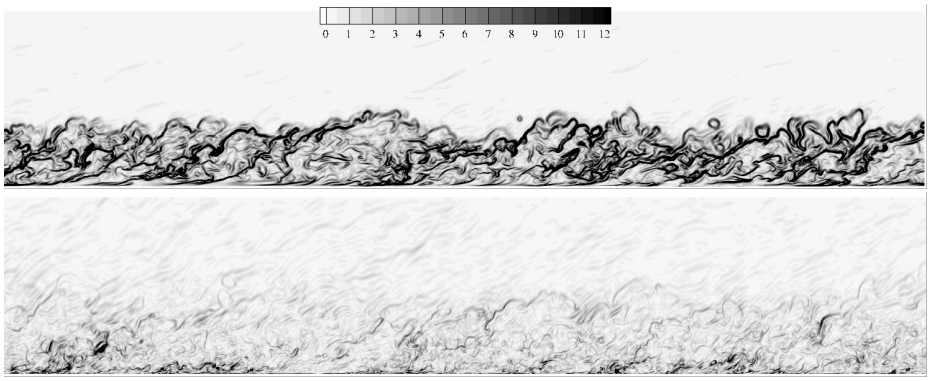

Fig. 6. Instantaneous sanpshots of normalized numerical Schlieren $|\nabla\rho|/(\overline{\rho}/\delta_{99,\mathrm{end}})$ for PFG (top) and DG (bottom).

property variations play a crucial role at all flow regimes. Temperature variations are negligibly small throughout the flow field and friction heating is very small even at hypersonic conditions: as a consequence, both the laminar and turbulent velocity profiles remain very close to the incompressible ones. However, strong compressibility effects do exist and, due to the peculiar variation of the sound speed in dense gases, they deeply affect the boundary layer stability properties: a supersonic radiating mode appears, while the Tollmien-Schlichting mode is stable. The DG turbulent region is characterized by higher local incompressible Reynolds numbers, due to the liquid-like behavior of the viscosity. This leads to higher turbulent intensities and higher turbulent and fluctuating Mach numbers than in PFG. Despite this, sheet-like compression structures characterizing the external region of the PFG boundary layer are much rarer in DG, while intense density gradient spots appear in a region close to the turbulent kinetic energy peak. Further work will focus on better characterizing the flow structures and analyzing noise generation. Assessment of turbulence models is also planned.

Acknowledgements: *This work was granted access to the HPC resources of IDRIS and TGCC under the allocation 2018-7332 made by GENCI (Grand Equipement National de Calcul Intensif). We also acknowledge TGCC for awarding access to the Joliot-Curie supercomputer under the allocation "Grands Challenges" gch032.*

Bibliography

[1] Thompson, P.A., *Phys Fluids*, **14** (9), 1843–1849 (1971).
[2] Sciacovelli L., Cinnella P., Grasso F., *J Fluid Mech*, **800**, 140–179 (2016).
[3] Sciacovelli L., Cinnella P., Grasso F., *J Fluid Mech*, **825**, 515–549, (2017).
[4] Sciacovelli L., Cinnella P., Gloerfelt X., *J Fluid Mech*, **821**, 153–199 (2017).
[5] Mack L.M., Boundary-layer linear stability theory, *AGARD TR 709* (1984).
[6] Franko K.J., Lele S.K., *Journal of Fluid Mechanics*, **730**, 491–532 (2013).
[7] Sciacovelli L. et al., Numerical investigation of supersonic dense-gas boundary layers, 2nd NICFD Conference, Bochum, Germany, 4-5 October 2018.
[8] Samtaney R., Pullin D. I., Kosovic B., *Physics of Fluids*, **13**, 1415 (2001).
[9] Duan L., Beekman I., Martin M., *J Fluid Mech*, **672**, 245–267 (2011).